N00014-72-C-0092
ADL 74010

CHARACTERIZATION OF IR WINDOWS
SEMIANNUAL TECHNICAL REPORT

by

J. S. HAGGERTY, E. T. PETERS

prepared for

OFFICE OF NAVAL RESEARCH
DEPARTMENT OF THE NAVY

sponsored by

ADVANCED RESEARCH PROJECTS AGENCY

JULY 1972

Arthur D Little, Inc

SEMIANNUAL TECHNICAL REPORT

"Form Approved Budget Bureau No. 22-R0293"

Program Title: Characterization of IR Windows

Contractor: Arthur D. Little, Inc., Cambridge, Massachusetts

Principal Investigator: John S. Haggerty 617-864-5770

Scientific Officer: Director, Physics Programs
Physical Sciences Division
Office of Naval Research
Department of the Navy

Contract Number: N00014-72-C-0092

ARPA Order Number: 1806/04-09-71

Program Code Number: S2202A

Effective Date of Contract: 71 October 01

Contract Expiration Date: 72 September 30

Amount of Contract: $47,533 (plus fee)

Sponsored by

Advanced Research Projects Agency
ARPA Order No. 1806/04-09-71

I. INTRODUCTION

High resistivity GaAs has usually been observed to have an optical absorptivity within the range 0.01 to 0.025 cm^{-1} at 10.6μm. This range does not appear to be affected by any of the intuitively important parameters--growth procedure, charge compensation element, crystallographic orientation, chemical purity or structural perfection. This suggests that:

a. The intrinsic absorptivity of GaAs at room temperature and 10.6μm radiation is of the order of $10^{-2}cm^{-1}$, or

b. There is some type of defect or structural disorder common to all charge compensated GaAs which is insensitive to variations in process parameters and which prevents the attainment of lower absorptivities.

The detailed characterization study undertaken by Arthur D. Little, Inc., under this contract is expected to resolve this issue, utilizing experimental methods that permit the detection of structural and compositional variations within a size range of 10^{-7} to 10^{-2}cm. Procedures emphasize direct observation of structure rather than analytical approaches; we expect to evaluate the size range of interest through selected combinations of optical and infrared microscopy, reflection and transmission X-ray topography and transmission electron microscopy. Our ultimate objective is to eliminate defects affecting the optical absorptivity of GaAs by appropriate modifications of crystal growth procedures.

Evaluation samples have been supplied by Bell & Howell who, under a concurrent ONR-sponsored program, is striving to prepare high quality, low absorptivity GaAs boules with an eventual goal of achieving scale-up to 3 to 12 inches in diameter. They are attempting to minimize absorption through selected variations in growth parameters, including dopant, concentration, growth rate, seed orientation, etc. Bell & Howell is conducting chemical analysis (spark source mass spectrometry) and absorption coefficient measurements on each boule prepared. The 1-cm thick cross section of each boule that is employed for the absorption measurement is subsequently being supplied to ADL for structural characterization.

By the end of the second quarter, five samples, having absorption coefficients ranging 0.013 to 0.031 cm^{-1}, had been received. As reported previously,[1] preliminary examination of these samples was conducted by back reflection X-ray topography. Most of the crystals displayed evidence of coring and faceted crystal growth. Other observed structure was associated with surface polishing and sample handling damage. These results are summarized in Table I. During the second quarter, further work has been conducted to elucidate the nature of bulk defects in these crystals. For this purpose, thin sections were prepared and transmission X-ray topographs obtained. Comparisons between optical, back reflection topographic and transmission topographic structures are presented in this report. In addition, attention was addressed to selecting an optimum film emulsion and determining suitable exposure and processing conditions to achieve maximum image resolution. Evaluation of various procedures for removing surface damage have also been conducted. The results of this work are described in the following section.

II. DEVELOPMENT OF EXPERIMENTAL METHODS

In order to observe the inherent structural perfection of the piece under examination, it is necessary to be able to recognize artifacts that have been introduced as a result of the experimental procedures that are employed. As a result, considerable attention has been directed during the past reporting period to optimizing the recording and presentation of topographic images as well as to sample preparation procedures, including cutting, thinning and polishing. Our conclusions are presented in the following sections.

A. X-ray Patterns

1. Image Recording

Of the various recording emulsions available, nuclear tracking plates appear to provide the best performance in terms of resolution and exposure time. By comparison, high contrast copy film and microfilm require four to six times longer exposure with equivalent or lower resolution. Glass bases for supporting the emulsion were vastly superior to normal polyester bases. The plastic bases deformed under the intense illumination of high magnification transmission optical microscopy. After surveying the properties of these other films, we limited our evaluation to Ilford L4 Nuclear Research Emulsion plates, having a mean AgBr diameter of 0.14μm and emulsion thicknesses of 25 and 50μm. For a 50% AgBr loading in the emulsion, these thicknesses reduce the intensity of CuK_α radiation by 40 and 75%, and of AgK_α radiation by 10 and 20%, respectively. With other conditions held equivalent, the 50μm emulsion can therefore be exposed in 1/4 to 1/2 the time required for the 25μm emulsion. Back reflection (422) topographs of a (111)-oriented GaAs slice obtained with both thicknesses of emulsion were found to yield equivalent resolution. After processing, the 50μm emulsion is approximately 10μm thick. All sample evaluations presented in this report have been conducted with 50μm emulsion L4 plates.

Several exposures were made to determine the effect of tube voltage on resolution. For this purpose, a (422) reflection from GaAs was limited

by slits to an area of about 1/8 x 1/4 inch. Exposures were made at 35kV and 20kV tube voltage. The crystal was then rocked off peak, and an adjacent set of exposures was made, representing background scatter from the sample. Representative photographs from this series are presented in Figure 1. Individual photographic emulsion "grains" can just be observed in the background images at 375X and are more clearly presented at 865X. For the most part, these grains have an apparent size of 0.5 to 1μm, or about three to seven times larger than the mean AgBr particle size. This is apparently the result of an X-ray photon causing the sensitization of several AgBr particles within a small volume rather than continuing activation to a single particle. There are some clusters of grains that are larger, i.e., 2 to 3μm in extent, indicated by arrows marked "a". The presence of an isotropic defect, such as a spherical precipitate, would therefore not be clearly identified unless it generated a strain field at least 5 μm in extent. Lineal defects, however, such as the polishing scratches shown in the left hand photographs, are clearly discernible at high magnification, as shown in Figure 1c. Even with an apparent limit in plate resolution of a few microns, these very fine, two-dimensional features, some of which are indicated by arrows marked "b", can be clearly observed. Figure 1c, obtained with a 20kV X-ray beam, is observed to exhibit the same resolution characteristics as the images obtained with a 35kV beam. The increased number of higher energy photons which are scattered at 35kV have no observed deleterious effect on resolution, thus permitting shorter exposure times.

2. Plate Processing

Several procedures for processing plates have been given in the literature. These have been reviewed by Meieran.[2] We have processed a series of similarly exposed plates by several procedures in which time, temperature and developers have been varied. The following were found to be best for Ilford Plates.

Presoak in distilled water (10-12°C) for 5 minutes.
Develop in fresh Kodak D-19 (10-12°C) for 20-30 minutes.
Rinse in distilled water (10-12°C) for a few minutes.

Fix in hypo (diluted 1:1 with distilled water at 10-12°C) for 20 minutes, or until clear.

Fix in full strength hypo containing hardener at room temperature for 30 minutes.

Wash for 1 hour in distilled water and dry.

The procedure is essentially the same as that suggested by Meieran.[2] Abrasion marks can be removed by soaking in water, then in 1% acetic acid, followed by gentle swabbing with cotton. The plate should then be washed and dried. Surface fog can be removed (or an overexposed plate can be lightened) by a standard reducing agent, such as Farmer's Reducer.

To assure highest plate quality, solutions should be freshly prepared, using high resistivity, filtered water. The water used to process these plates had a resistivity in excess of $2 \times 10^6 \Omega$cm and was passed through a 0.2μ filter. Drying should be carried out in a dust-free enclosure.

Since topographic images are recorded at about a 1:1 magnification, enlargements are necessary to observe the detailed image structure. Although we have not evaluated all procedures described in the literature, we have achieved consistent results utilizing Polaroid Type 55 P/N film to record transmitted light microscope images at 4 to 1040X magnifications. Photographs are then printed on high contrast paper (F4 to F6) with no more than a two- to three-time enlargement from the Polaroid negative.

B. Sample Preparation

Thin samples, on the order of 3 mils and 100A thickness, are required for transmission X-ray topography and transmission electron microscopy, respectively. It is imperative that all surface damage introduced during the preparation of the thin section be removed prior to examination. The presence of surface artifacts could lead to misinterpretation of the inherent structure of the sample.

Consequently, the extent of induced surface damage was evaluated after various processing steps, including cutting, mechanical polishing and chemical and molecular thinning. The degree of damage was evaluated by edge topographs of (110) cleavage faces normal to the surface of the sample, utilizing (440) back reflection topographs. The procedure has been described in detail by Rozgonyi and Haszko.[3] Six surface conditions have been evaluated as follows.

I. As-received polish from Bell & Howell*

II. As-cut, utilizing a wire saw with a 0.010-inch diameter stainless steel wire blade and 600 grit SiC in glycerine abrasive.

III. As-cut, followed by removal of 0.010 inch thickness by mechanically polishing on 600 grit SiC paper.

IV. Same as III, followed by mechanical lapping on silk with 6μ diamond and then with 1μ diamond.

V. As-cut, followed by mechanical lapping on silk with 6μ diamond and then with 1μ diamond.

VI. Same as IV, followed by removal of 0.003 inch of material by argon sputtering.

The results of these evaluations are shown in Figure 2. (Roman numerals correspond to preceding surface treatments.) Surprisingly, there is not a great deal of difference observed for the various mechanical polishes. In all cases, damage is less than 0.001 inch or 25μm. The ion thinned (sputtered) sample shows no evidence of surface damage and is clearly the preferred surface condition.

Based on this work, it is imperative to remove the final 0.001 inch of surface by ion sputtering to assure elimination of surface artifacts.

---

*The Bell & Howell preparation procedure includes cutting on an ID diamond saw, grinding on 600 and 1200 grit SiC and mechanically polishing on silk with alumina (Linde A and B) abrasive.

III. CHARACTERIZATION OF GaAs SAMPLES

Sample slices from five (111)-axis GaAs boules submitted by Bell & Howell were previously surveyed by back reflection X-ray topography methods.[1] On a gross scale, two samples (Nos. 1852T and 2602-10) exhibited uniform images, whereas two of the other samples (Nos. 1860T and 1860B) exhibited considerable strain damage which was attributed to faceted growth and coring; the fifth was intermediate. There was no correlation between the measured absorption at 10.6μm radiation and gross imperfection. The data presented in Table I show one of the better samples, on the basis of structure, to have the highest absorption coefficient. Therefore, if a structural defect is responsible for the persistently high absorption coefficient, it is common to all of these samples.

A. Experimental Procedures

We utilized techniques during the past quarter which permit a higher magnification view of the prevailing internal defect structure in these samples. As shown previously, the image from back reflection topographs originates from the first 0.001 inch or so below the sample surface. Unless special surface preparation is used, this layer is heavily damaged as a result of sample cutting and polishing and therefore is not representative of the bulk sample. Thin slices (about 0.003 inch thick) from each sample were prepared using the procedures described in the previous section to remove all surface damage. These were employed for complementary examinations by oblique illumination surface photography, back reflection X-ray topography and transmission X-ray topography. It is intended that the same pieces will also be examined by infrared transmission microscopy and transmission electron microscopy.

The slices approximated longitudinal sections of the initial boules; each slice was oriented to a (111) face with edges corresponding approximately to (110) and (211) faces. The sections were made at approximately the boule diameter so radial variation of defect density and type was revealed. Preparation included cutting with a wire saw, removal of about 0.004 inch from each side on 600 grit SiC paper, diamond polishing and finally ion thinning to a final thickness of about 0.003 inch.

TABLE I

MEASURED PARAMETERS ON GaAs CRYSTALS SUPPLIED BY BELL & HOWELL

Sample No.	Axis Orientation	Resistivity ($X10^6$ ohm-cm)	Absorption Coefficient (cm^{-1})	Gross Structure
1852T	<111>	35	0.031	Uniform
1857T	<111>	25	0.013	Slight Faceting
1860T	<111>	90	0.018	Faceting
1860B	<111>	90	0.019	Heavy Faceting
2692-10	<111>	50	0.016	Uniform

One of the samples (No. 1857T) thinned at an anomously high rate and had a final thickness of approxiately 0.0005 inch. This sample was too fragile to handle and was not utilized. Also, sample Nos. 1860T and 2602-10 fractured along (110) cleavage planes normal to the surface plane; for these cases, the largest part of the slices were examined.

B. Results

1. Ion Polished Surfaces

Initial characterization included visual examination of the surfaces by optical and scanning electron microscopy. In all cases, the ion thinned samples contained numerous shallow craters of varying diameter, as shown in Figure 3. Impingement of craters occurred frequently; in some cases, impingement was limited to two or three adjacent craters (labeled A in Figure 3); whereas in other cases, impingement was strung out along a line (labeled B). These same features are shown at higher magnification in Figure 4a. The edge of the sample, shown in Figure 4b, is apparently influenced by deposition and resputtering of copper from the heat sink substrate, resulting in the characteristic cone structures. Occasionally cones were obserced in craters away from the sample edge.

At present, we have no understanding of why craters form. They are apparently the result of preferential sputtering at specific points, which then widen spherically. They become evident (25X optical microscopy) only after approximately 8μm of material has been sputtered off. One can speculate that craters originate at point defects, i.e., regions of high strain (such as dislocation cores) or chemical inhomogeneity (precipitates). Were this the case, the largest craters would be expected to be the earliest formed (that is, nearest to the original surface). However, the lineal arrays of craters, which are reminiscent of polishing scratches on the original surface, are generally formed from fairly small diameter craters. Rather than pursue a thorough understanding of the ion thinning process at this time, we intend to compare the distribution of surface craters to other structural features that are observed by X-ray topography, infrared microscopy and electron microscopy. Consequently, surface photographs of crater distributions were obtained from three of the thinned GaAs slices at several magnifications. These photographs will be presented together with the X-ray topographic data.

These slices were employed for (440) back reflection and (220) transmission X-ray topographs. The back reflection patterns were obtained by the experimental procedure presented in the last report,[1] and transmission patterns taken with AgK_α radiation, utilized the geometry presented in Figure 5.

2. Characterization of Individual Samples

Optical photographs and X-ray topographic images of the ion thinned slices are presented for sample Nos. 1860B, 1852T, 2602-10, and 1860T in Figures 6 through 9, respectively. The higher magnification views are taken in the central region of the corresponding lower magnification shots, except as noted in the text. The optical photographs were obtained from the side of the sample corresponding to the transmission topograph beam exit face which was also the face examined by reflection topography. In this way direct comparison of image features could be conducted.

In review, the observed optical images result from differences in light scattering, generally due to variations in surface topography. The X-ray images are generated as a result of diffraction enhancement from localized regions of the sample that are strained. Such strain is caused by the breakdown of a regular lattice structure due to point and line defects (dislocations, vacancies, stacking faults, slip lines), chemical variations (precipitates, segregation) and residual stresses generated during crystal solidification and cool down to ambient temperature. Other factors which contribute to the dynamical X-ray image can be ignored at present. The craters are too shallow relative to the thickness of the sample to image due to absorption.

Sample 1860B ($\alpha = 0.019\ cm^{-1}$)

Optical and transmission X-ray topographs are presented at several magnifications in Figure 6. The low magnification optical image displays many lines, designated by A, is shown at several magnifications. It is noted at high magnification that the line set actually corresponds to quite small, connected craters. Individual craters range in size from sub-micron to about 100 microns in extent.

Other than one deep polishing mark, labeled B in the low magnification photograph and topograph, there are no obvious similarities in structure between the optical and X-ray images. The foreshortening of the X-ray image in the horizontal direction results from the diffraction geometry.) At low magnification, the X-ray image shows substantial structure reminiscent of the previously presented back reflection topographs.[1] The apparent change in film density across the line marked C is the result of a composite exposure which was required to image the entire crystal. Other variations in density are the result of severe inhomogeneous lattice strain. At higher magnification (22X), the structure is observed to consist of very small cells. Even at quite high magnification (150X), the structure is so dense that it is impossible to resolve individual defect features.

The observed structure is typical of that resulting from breakdown of a planar solid-liquid solidification interface to a cellular interface. Cell walls are sinks for impurities as well as dislocations causing these regions to be highly strained compared to the interior of the cells. This is the source of the enhanced X-ray diffraction contrast.

Sample 1852T ($\alpha = 0.031\ cm^{-1}$)

A similar series of optical and X-ray topographic images are presented for Sample No. 1852T in Figure 7. The optical images bear no resemblance to the corresponding X-ray topographic images, either in size or distribution. The X-ray topographs both exhibit a comparable cell structure throughout most of the cross section; the cell size is about 0.010 inch in diameter, more than an order of magnitude larger than the previous sample.

The back reflection image is developed from a thin surface layer corresponding to 20-25% of the sample thickness. As a result, the reflection image tends to contain less structure than the transmission image. The white and black spots on the reflection pattern (some of which are indicated by E) are artifacts caused by plate processing in aged solutions.

The low magnification transmission image shows a uniform cell structure throughout the section. The left and right hand ends of the image, corresponding to the periphery of the boule, additionally exhibit numerous lineal traces (noted by F) oriented parallel to the intersection of {111} planes with the wafer surface. These correspond to slip traces lying along <110> directions and are the result of strain accommodation by the lattice.

Sample 2602-10 (α = 0.016 cm^{-1})

Optical and X-ray images of Sample 2602-10 are presented in Figure 8. The right hand portion of the sample broke during sample preparation. The right hand edges of the low magnification images correspond to <110> cleavage faces. Approximately one-third of the sample is missing.

The high magnification optical photograph reveals a feature not seen in the other samples, namely, a series of wavey lines of connected, very small craters. Several of these are indicated by the letter C. It is interesting to note that this crater substructure is on the same size scale as the cell-type structure revealed by transmission topography.

The back reflection topography shows few features of interest. A very faint background structure is present (not clearly discernible in the photograph) which is generally similar to that shown by the transmission images. The white spots are artifacts from film processing.

In transmission, the left side of the topograph (corresponding to the outer periphery of the boule cross section) is observed to be heavily faulted in the same manner as Sample 1852T. This faulting is the result of slip in {111} planes along <110> directions and results from strain accommodation by the lattice. It is likely that the strain originated from residual stresses generated by differential cooling of the boule. The center of the sample is more uniformly cellular, with a cell size similar to Sample 1852T. Even in this region, some dislocations, indicated by the arrows in the 22X center image, lie along the active slip system.

Corresponding transmission images from (220) and (422) reflections are shown at 65X and 150X. Although the patterns are similar, all features are not in exact correspondence. For reference purposes, the letter J indicates equivalent positions on each topograph. The structure noted by L is sharp and clear on the (220) images, but missing from the (422) images. Likewise, the features marked N are present on the (422) images, but missing from the (220) images. These differences occur as a result of anisotropic strain in the lattice planes adjacent to a defect. In the case of a dislocation (either edge or screw), there is minimum distortion in the plane that contains the Burgers vector of the dislocation. A topography of this plane will not image the dislocation. Likewise, there is maximum distortion in the plane perpendicular to the Burgers vector, causing maximum image contrast for this plane. Formally, it can be stated that dislocations are not imaged when the following condition is satisfied

$$\vec{g} \cdot \vec{b} = 0$$

where $\vec{g}$ and $\vec{b}$ are the Burgers vector and the pole of the diffraction plane. Since both the (220) and (422) planes contain specific <110> directions, i.e., [110] and [011], respectively, some features as noted above, will be missing from the individual topographs.

These images, therefore, confirm the presence of dislocations having <110> Burgers vectors, and also reveal maximum contrast for the (220) image, as would be predicted. It is for this reason that we have utilized the (220) reflection for all transmission topographs.

The similarity of the substructure observed in the high magnification optical photograph with the cell structure observed in the X-ray images suggests that the pitting may be related to cell boundaries. The intercrater spacing is much smaller than the apparent interdislocation spacing observed with the transmission topographs. It should be noted that dislocations with specific Burgers vectors will not be imaged in any given topograph. The strain induced diffraction contrast observed is considerably higher than for the other samples, suggesting a less diffuse segregation of impurities in the vicinity of the cell walls.

Sample 1860T (α = 0.018 cm^{-1})

Transmission topographs of a portion of the thin section from Sample 1860T are presented in Figure 9. These topographs are included principally to show the generally improved structure of this sample, taken from the top of Boule 1860, compared to the structure shown in Figure 6, representing the bottom of the same boule. Even though the cell size of the two samples is approximately an order of magnitude different, the measured absorption coefficient is essentially identical.

IV. CONCLUSIONS

Transmission and back reflection X-ray topographic analysis of Cr-doped GaAs samples from Bell & Howell have revealed several characteristic defect structures. Samples grown by the hot-wall autoclave technique contained high residual stresses[1] resulting from growth facets, while the sample grown by liquid encapsulation appears esentially free of bulk residual stresses. In all cases, a cellular dislocation structure is evident, indicating breakdown of solidification interface stability. The cell size (10-200μm) and dislocation density vary considerably between individual crystals. Again, from this standpoint, the crystal grown by the liquid encapsulation technique was of superior quality. The cell size was approximately an order of magnitude larger than the poorest hot-wall autoclave sample. The bulk dislocation density in this crystal was between 10^2-$10^3/cm^2$ in the best regions. As expected, the cell structure of the last to grow end of the boule was smaller. In all cases, there was evidence of {111}, <110> deformation in the outer annuli of the crystals, probably resulting from relaxation of radial temperature gradients which existed in the boules during growth.

These topographic analyses have not revealed a defect that correlates with the optical absorptivity of 10.6μm. The highest absorptivity (0.03 cm^{-1}) was observed for a relatively good crystal (1852T) and the poorest crystal (1860B) exhibited an average absorptivity (<0.02 cm^{-1}). Thus, to date, these studies have failed to explain the unacceptably high residual absorptivity. They have revealed residual stresses in some crystals which will degrade their optical performance due to stress induced berefringence effects. Future work will emphasize higher magnification characterization techniques.

V. FUTURE WORK

We intend to examine the same sample slices reported on here by infrared microscopy and transmission electron microscopy. Previous inspection of thick slices of GaAs by IR microscopy were of limited value due to the very high absorption of 1μm radiation by the Cr-compensated material. Preliminary investigation of the thin sections shows transmission with selected absorption at defects.

Transmission electron microscopy is absolutely essential for carrying out a search for point defects, fine precipitates, etc. Samples will be thinned at MIT by ion bombardment.

We have received an additional set of sixteen samples from Bell & Howell representing differences in seed orientation, growth rate and position of sample within boule. These samples have absorption coefficients ranging from 0.010 to 0.021 cm^{-1}. Based upon back reflection X-ray topographs, several representative samples will be selected for thorough characterization by the methods described herein.

VI. REFERENCES

1. J.S. Haggerty and E.T. Peters, "Characterization of IR Windows," First Quarterly Technical Report, Arthur D. Little, Inc., March 1972, Contract N00014-72-C-0092.

2. E.S. Meieran, "X-ray and Electron Microscopy," Siemens Review XXXVII, Fourth Special Issue, 39-80 (1970).

3. G.A. Rozgonyi and S.E. Haszko, "Reflection X-ray Topograph of GaAs and GaP Cleavage Faces," J. Elec. Soc., 117, 1562-1565 (1970).

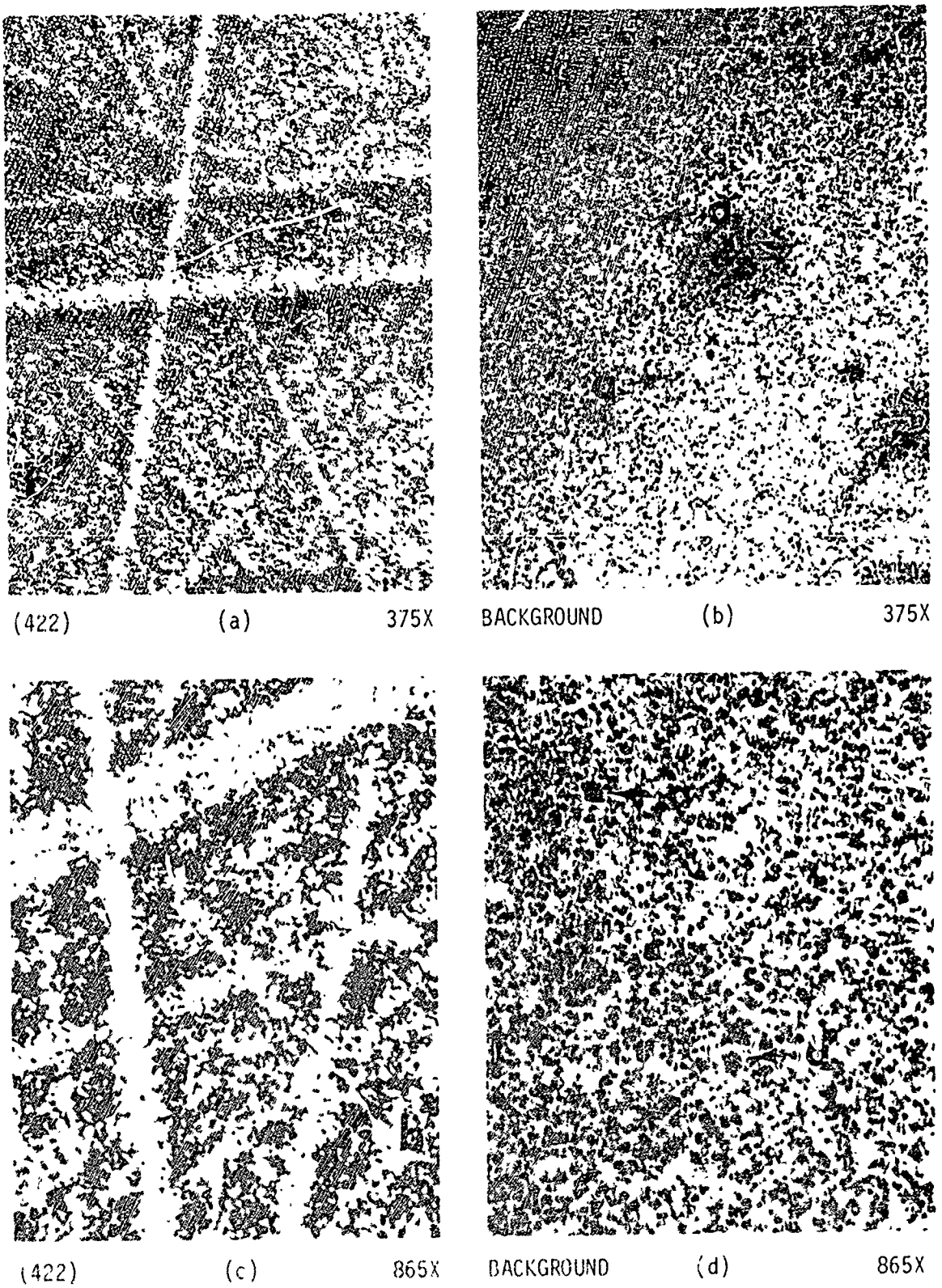

FIGURE 1 BACK REFLECTION TOPOGRAPHIC IMAGES FROM (111) GaAs, CuK$_{\alpha_1}$ RADIATION, TRANSMITTED LIGHT (a), (b), AND (d) 35 KV TUBE VOLTAGE, (c) 20 KV TUBE VOLTAGE

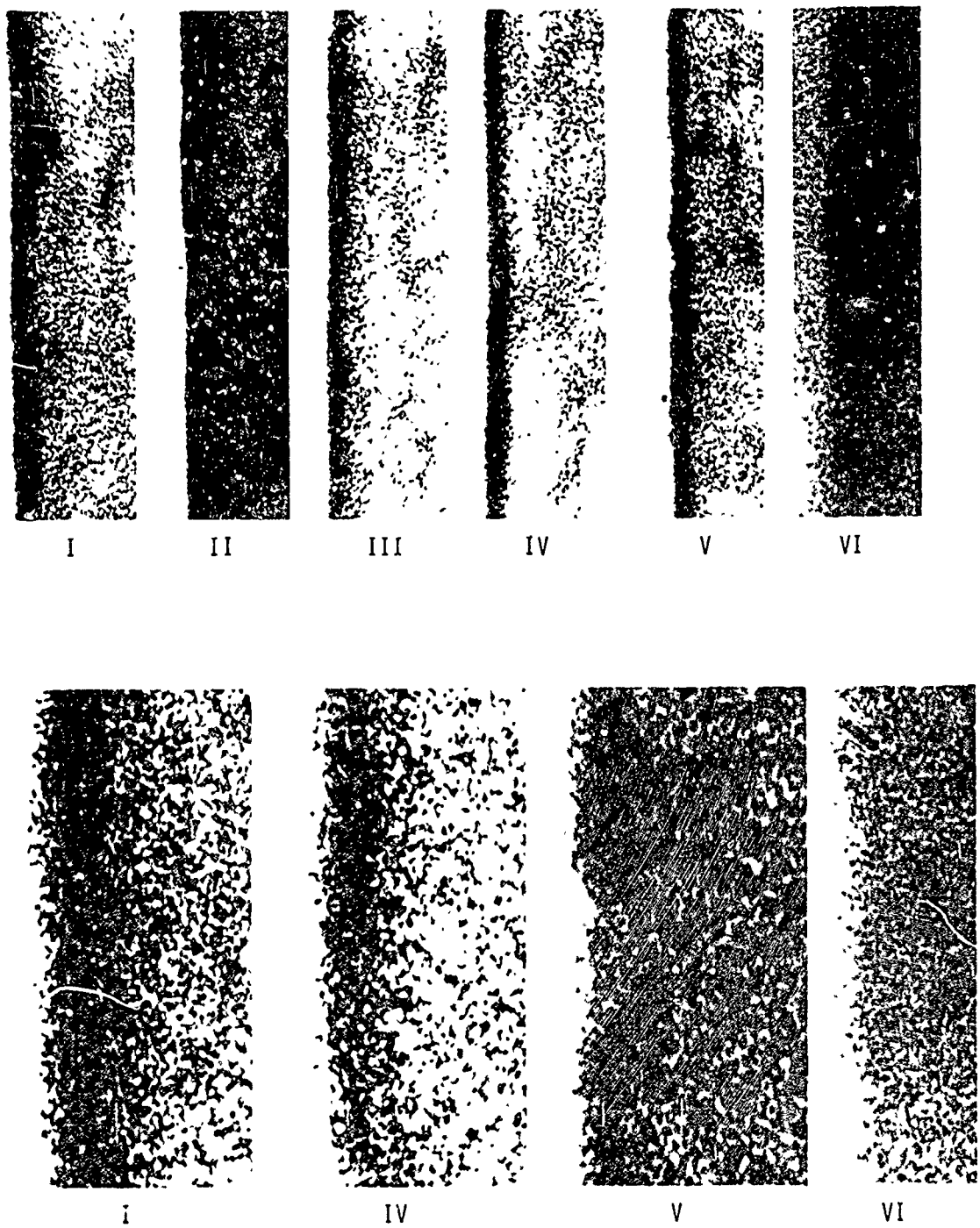

FIGURE 2 (440) EDGE TOPOGRAPHS OF (110) GaAs CLEAVAGE FACE AFTER VARIOUS SURFACE PROCESSING (ROMAN NUMERALS CORRESPOND TO TREATMENTS DESCRIBED IN TEXT). APPARENT MAGNIFICATION: TOP - 120X, BOTTOM - 500X

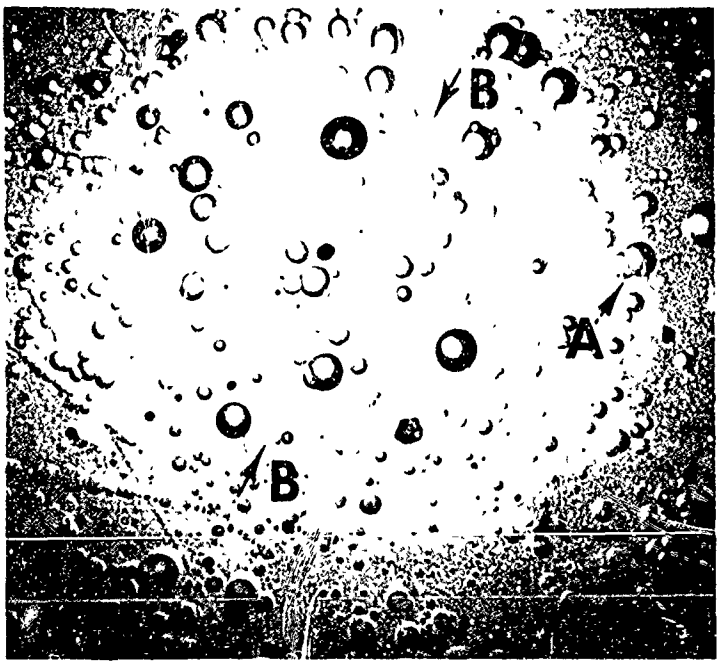

(a) 170X

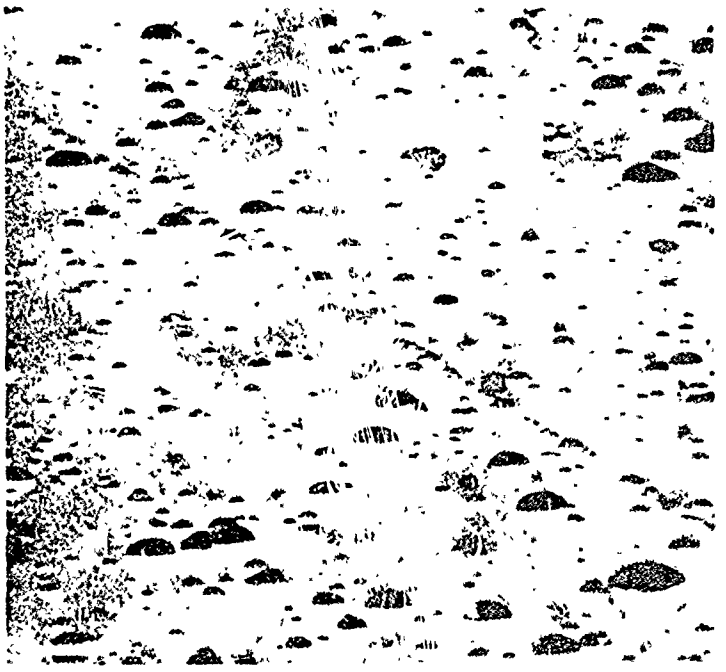

(b) 225X

FIGURE 3 PHOTOGRAPHS OF GaAs SURFACE AFTER ION THINNING (a) OPTICAL MICROSCOPY (b) SCANNING ELECTRON MICROSCOPY

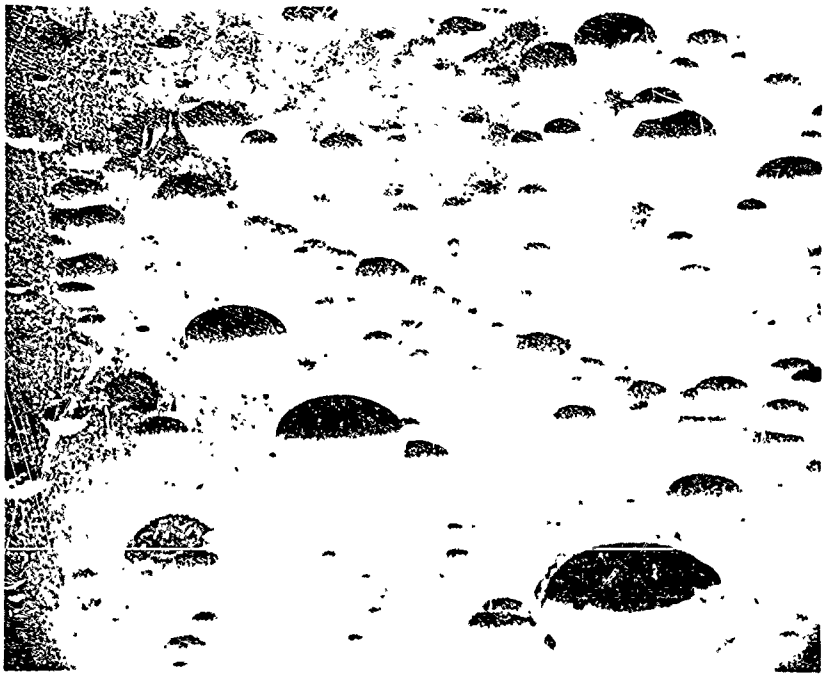

(a) 550X

(b) 2250X

FIGURE 4 SCANNING ELECTRON MICROGRAPHS OF GaAs SURFACE AFTER ION THINNING (a) CENTER OF SAMPLE (b) EDGE OF SAMPLE

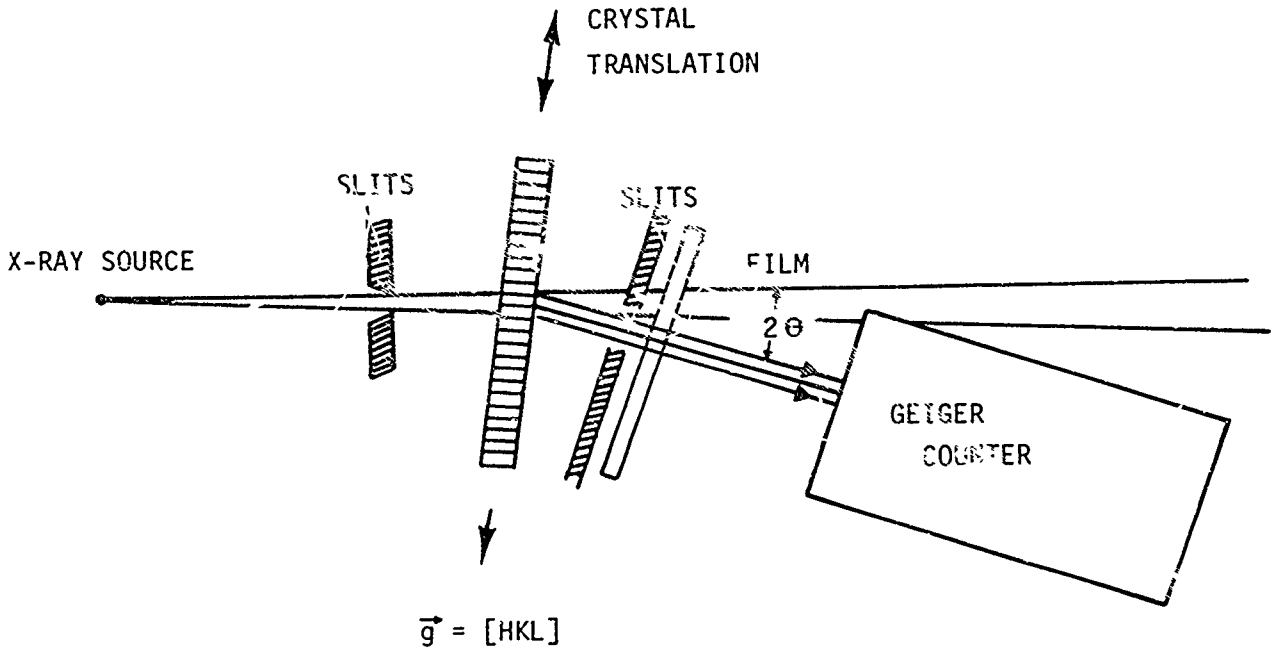

FIGURE 5 SCHEMATIC SKETCH SHOWING THE SCANNING TRANSMISSION TOPOGRAPH GEOMETRY

OPTICAL

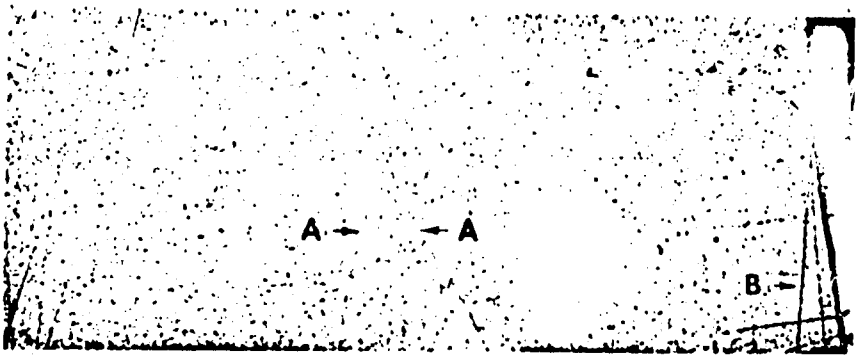

10X

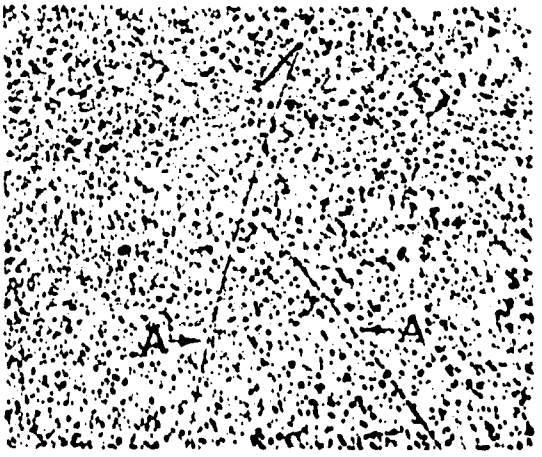

22X

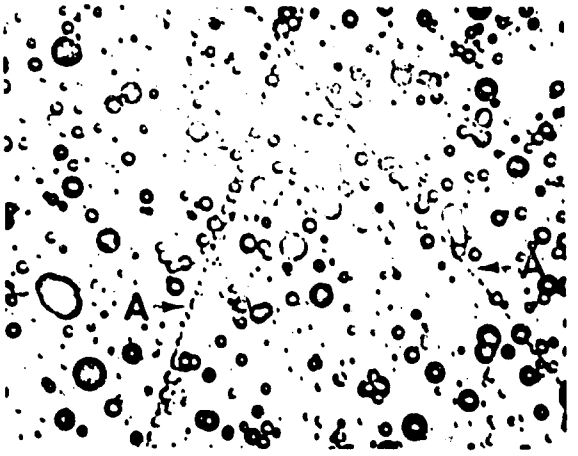

150X

X-RAY TRANSMISSION

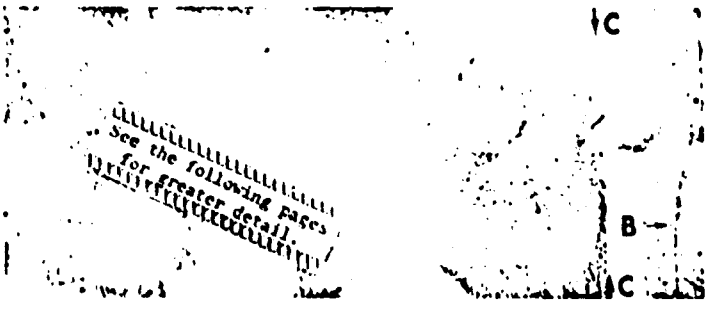

10X

22X

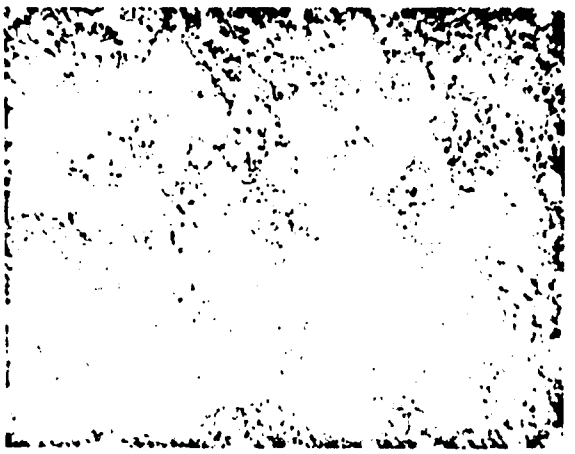

150X

FIGURE 6 OPTICAL AND TRANSMISSION X-RAY TOPOGRAPHS OF (111)-ORIENTED THIN SECTION OF GaAs FROM SAMPLE NO. 18609

OPTICAL

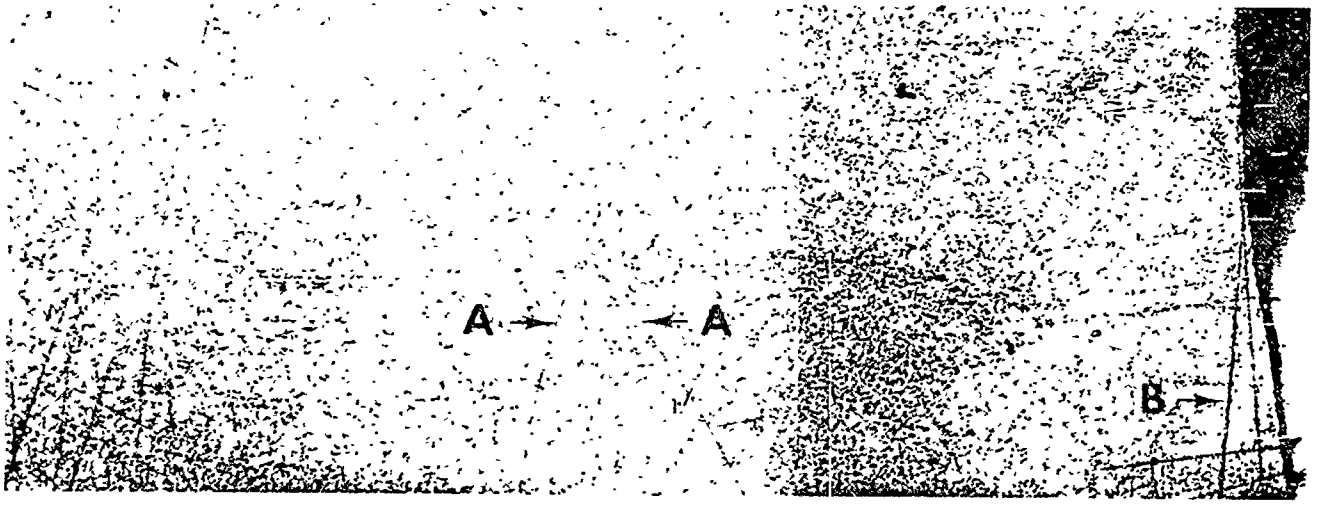

10X

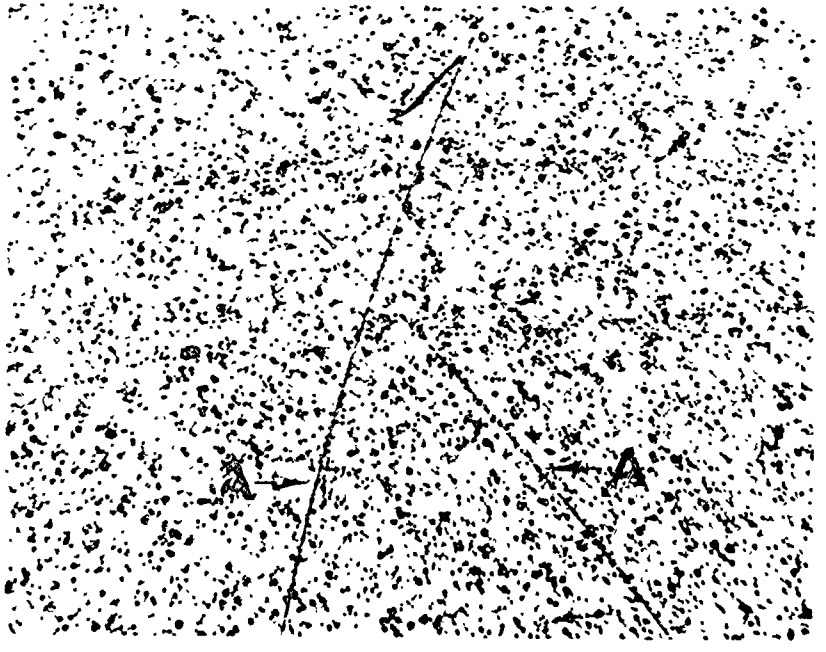

22X

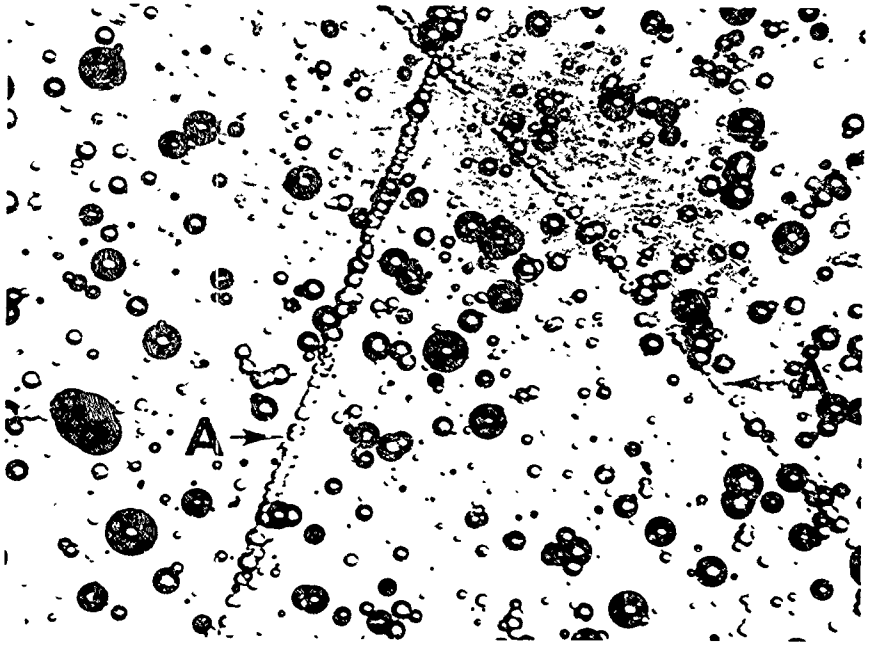

150X

X-RAY TRANSMISSION

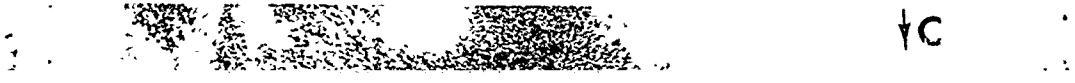

150X

X-RAY TRANSMISSION

10X

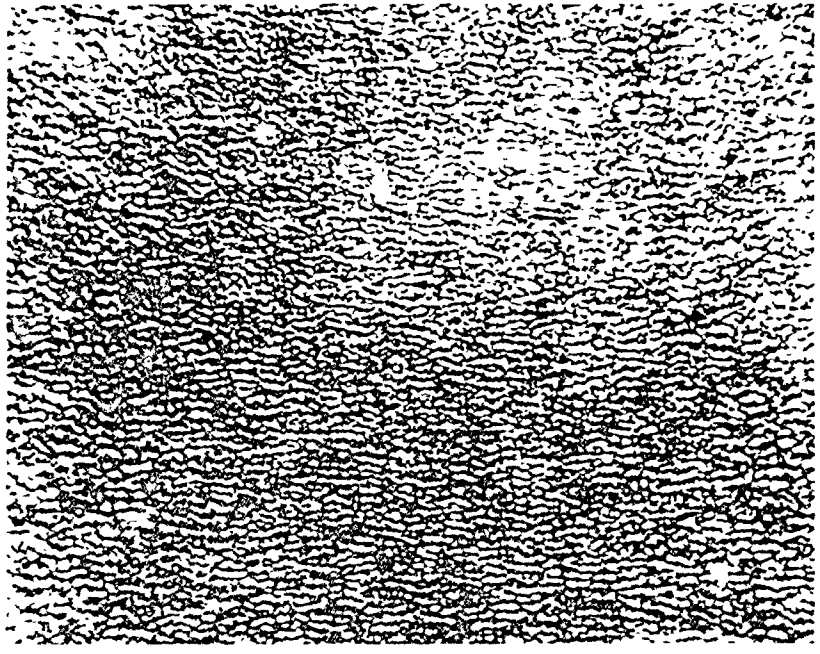

22X

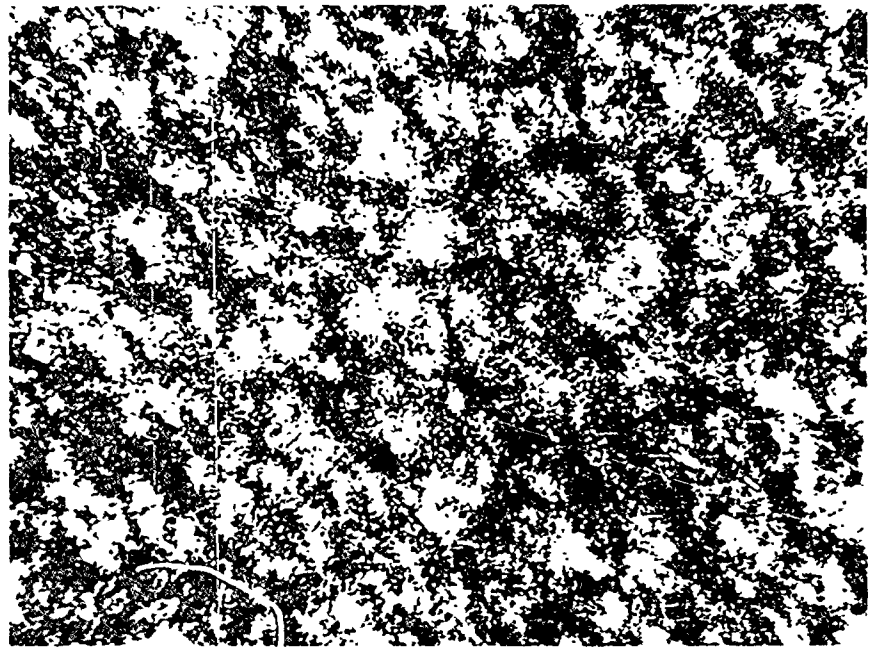

150X

FIGURE 6 OPTICAL AND TRANSMISSION X-RAY TOPOGRAPHS OF (111)-ORIENTED THIN SECTION OF GaAs FROM SAMPLE NO. 1860B

OPTICAL

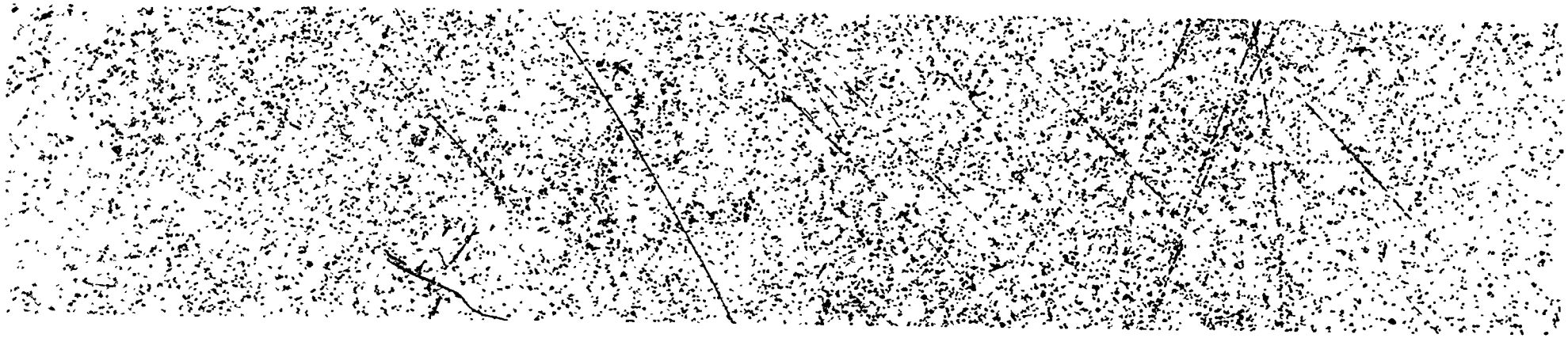

10X

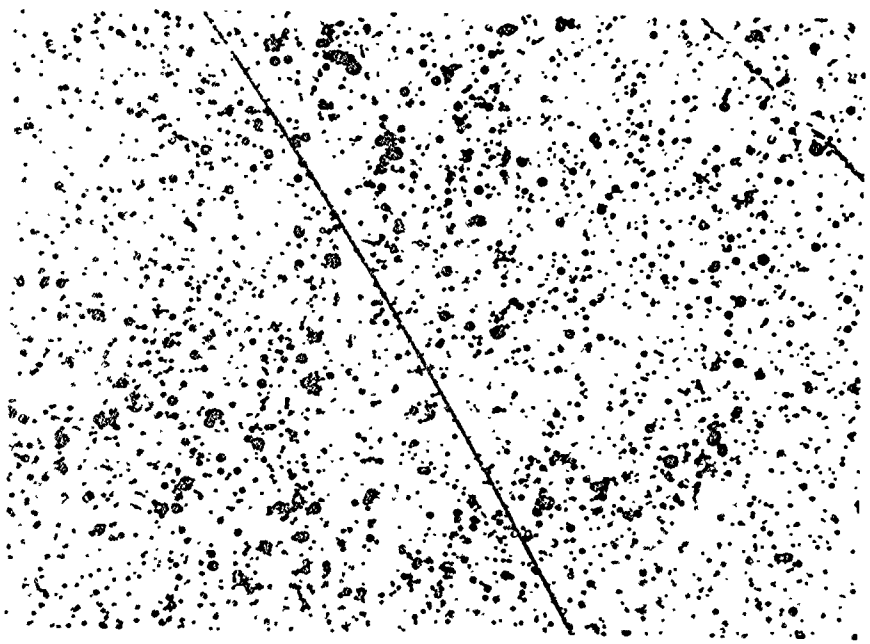

22X

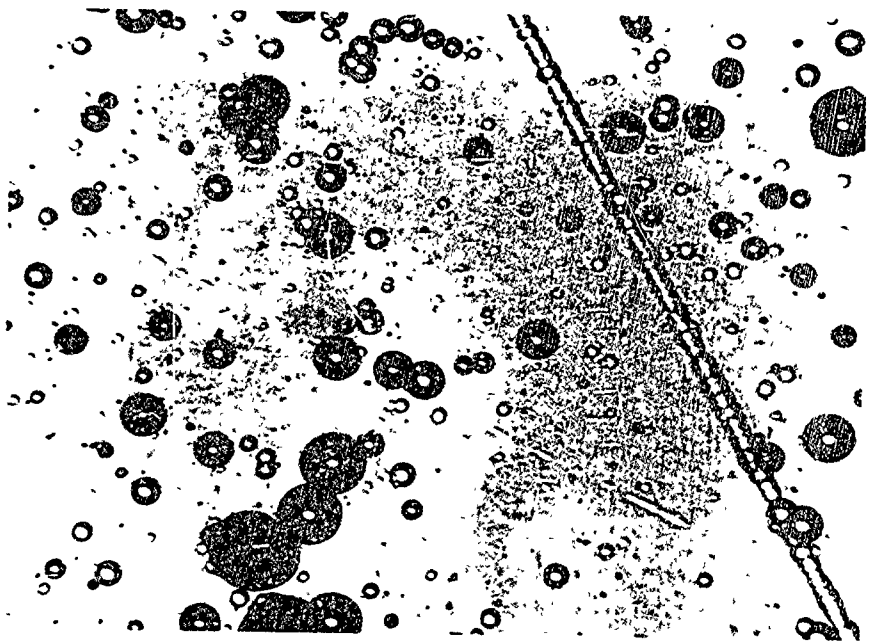

150X

X-RAY BACK REFLECTION

X-RAY BACK REFLECTION

10X

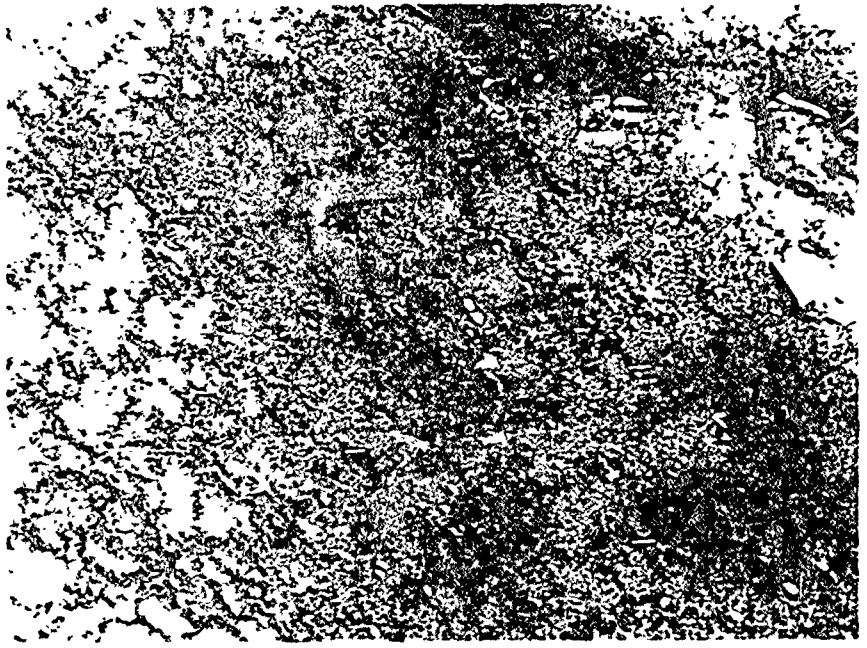

22X

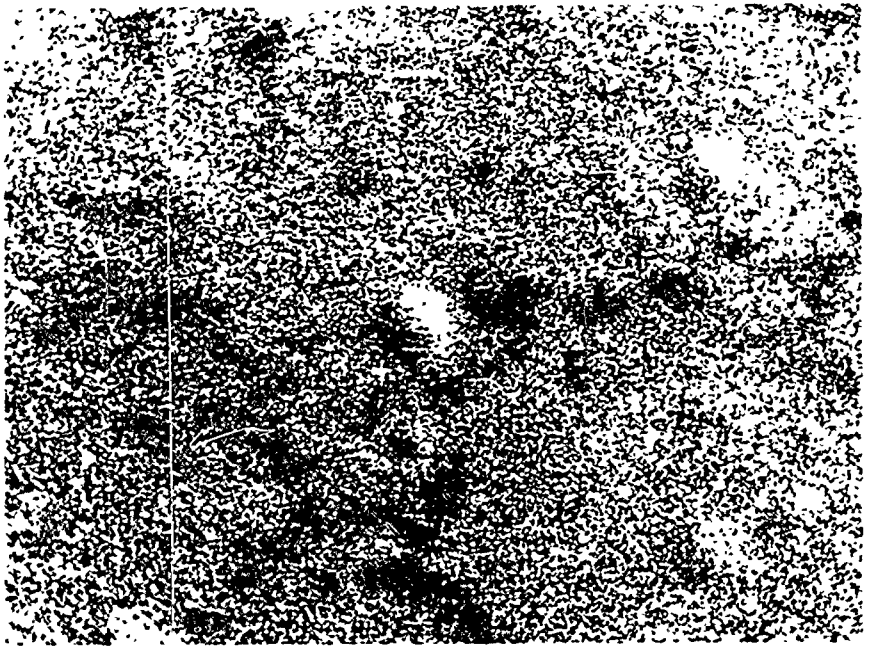

150X

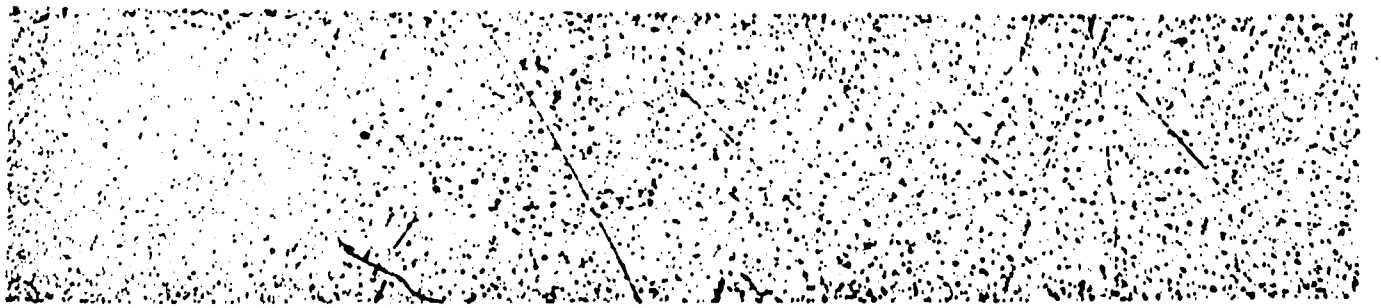

10X

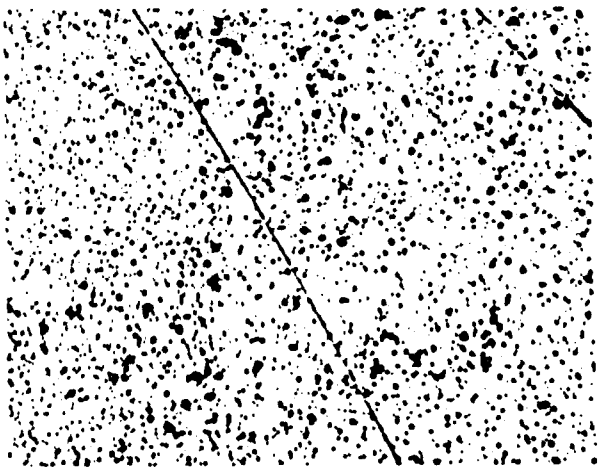

22X

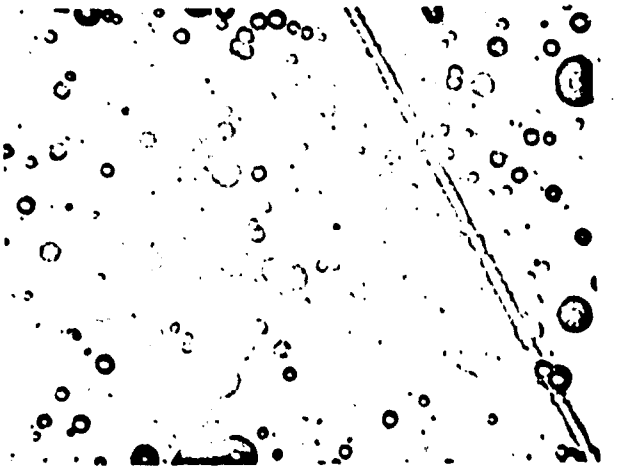

150X

X-RAY BACK REFLECTION

10X

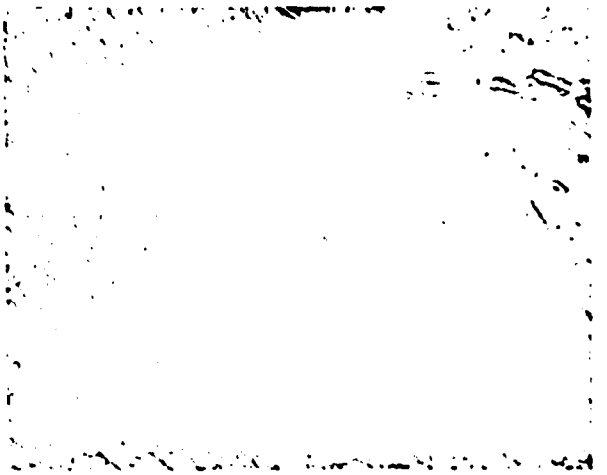

22X

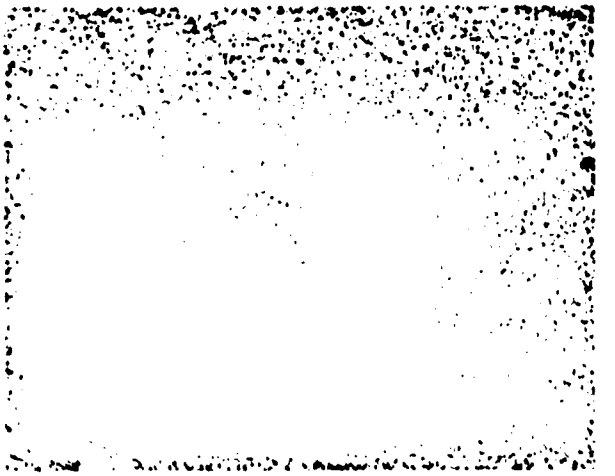

150X

X-RAY TRANSMISSION

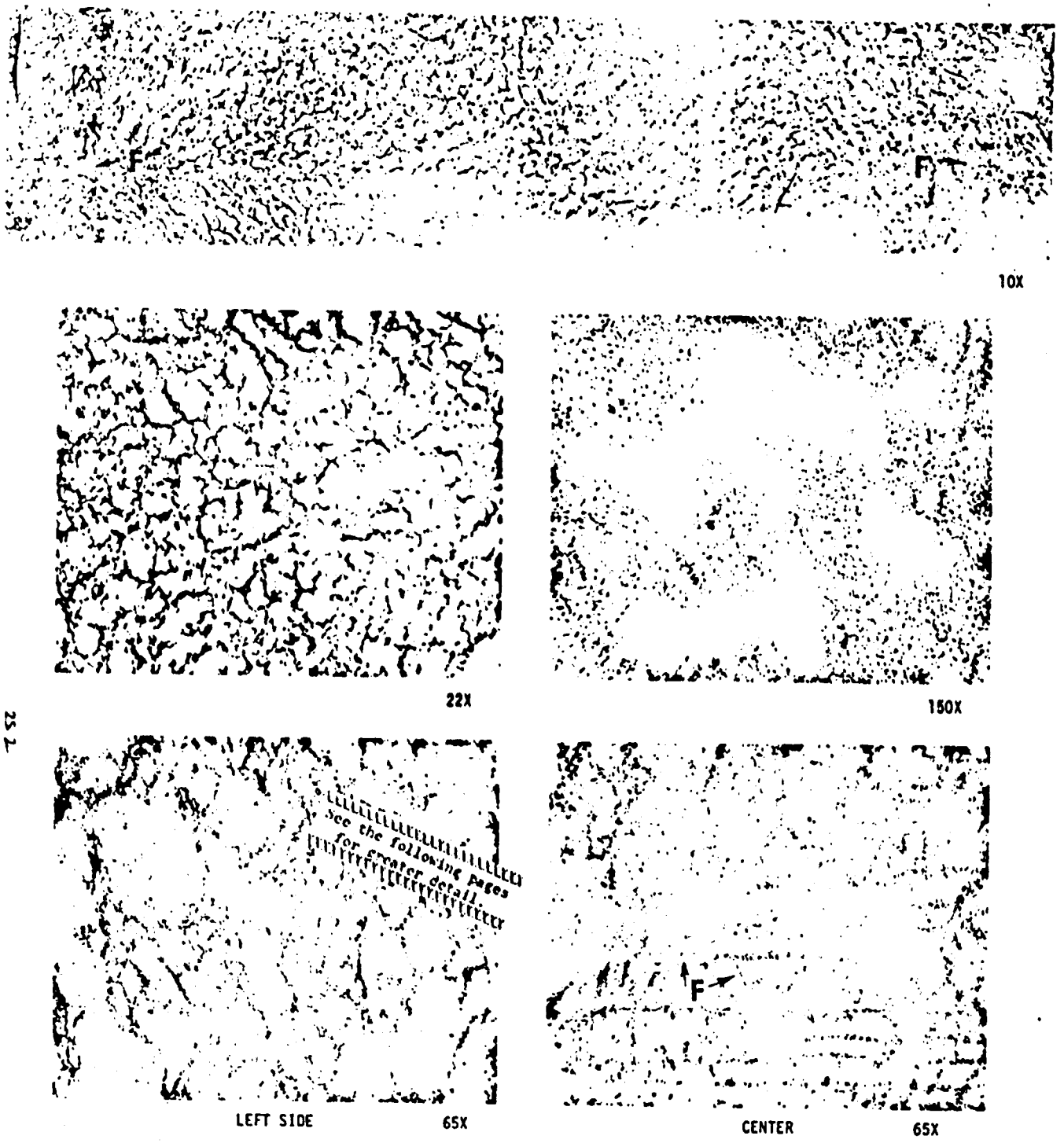

FIGURE 7 OPTICAL, BACK REFLECTION AND TRANSMISSION X-RAY TOPOGRAPHS OF A (111)-ORIENTED THIN SECTION OF GaAs FROM SAMPLE NO. 1852T

X-RAY TRANSMISSION

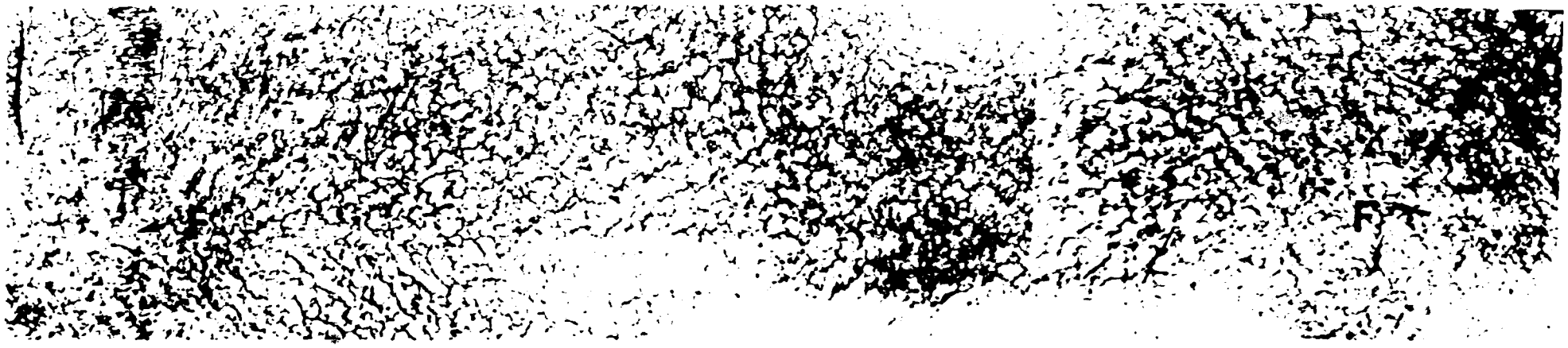

10X

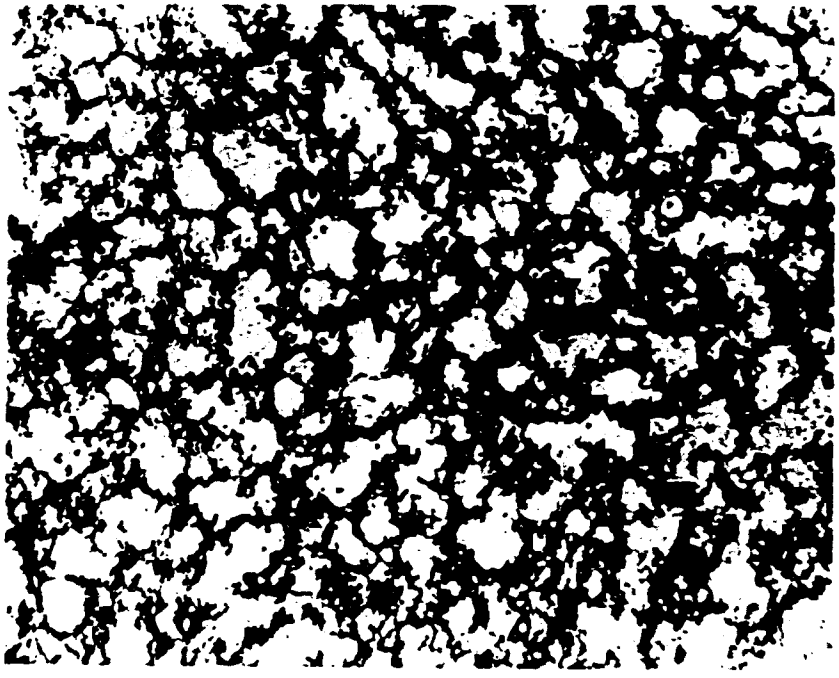

22X

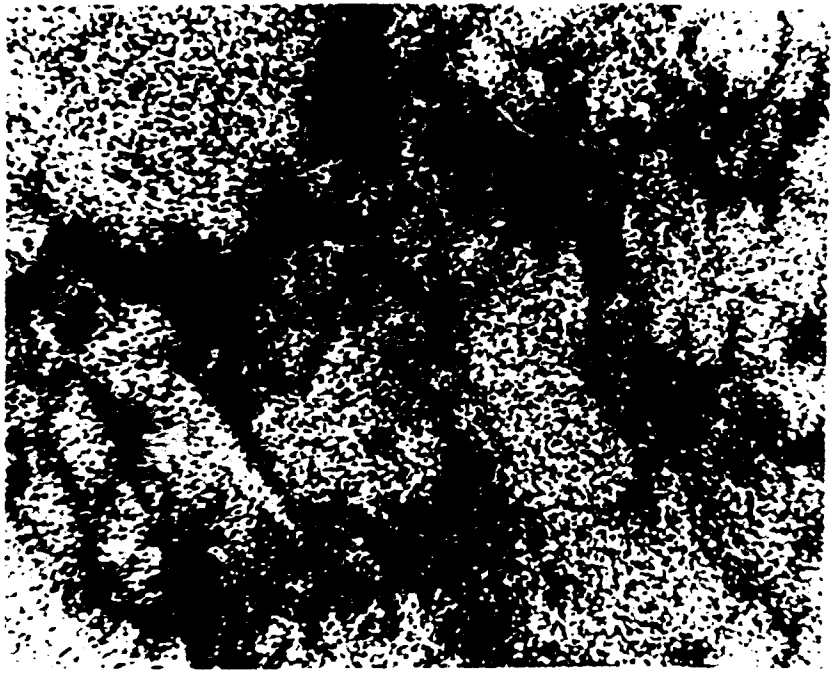

150X

22X 150X

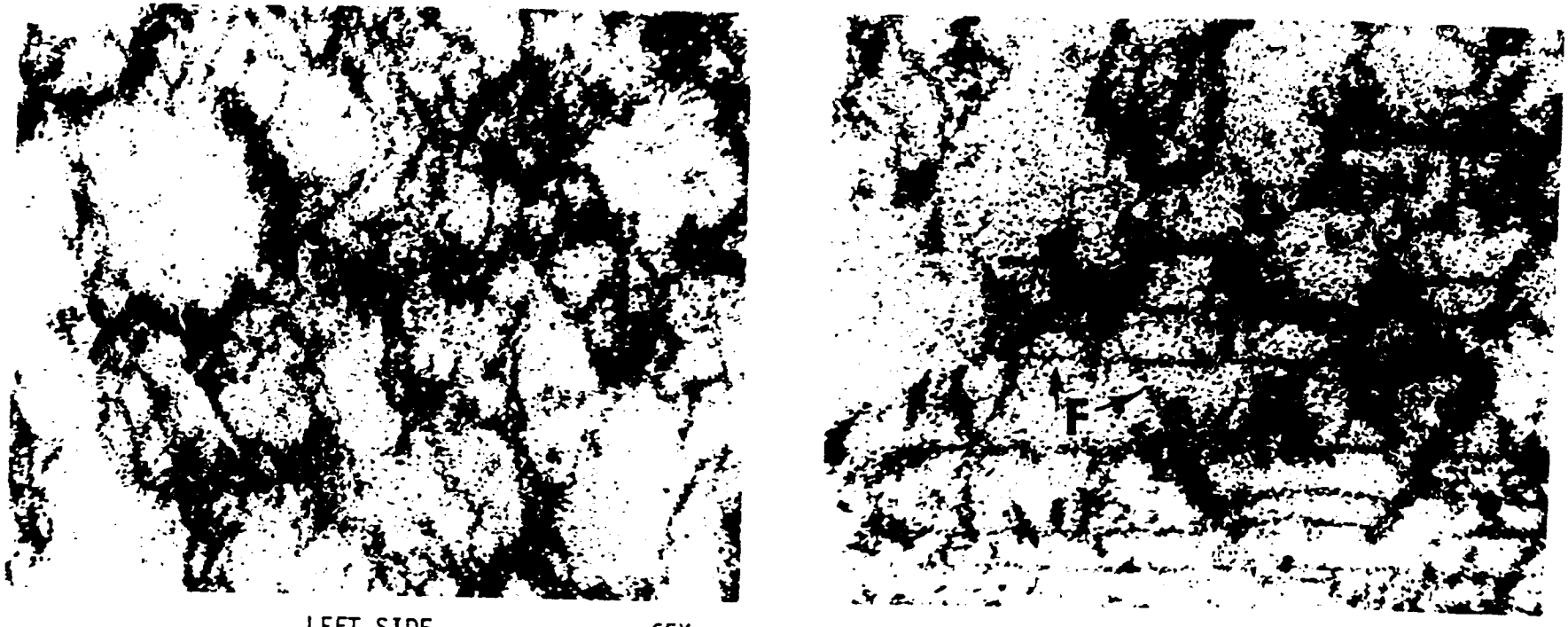

LEFT SIDE 65X CENTER 65X

FIGURE 7 OPTICAL, BACK REFLECTION AND TRANSMISSION X-RAY TOPOGRAPHS OF A (111)-ORIENTED THIN SECTION OF GaAs FROM SAMPLE NO. 1852T

10X

OPTICAL

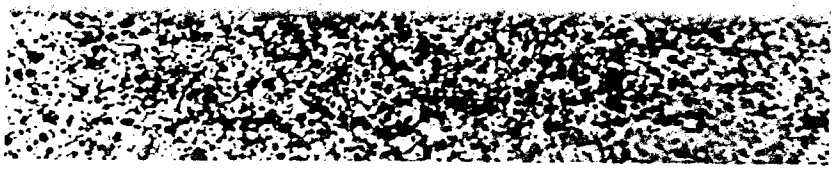

22X

150X

26.2

X-RAY BACK REFLECTION

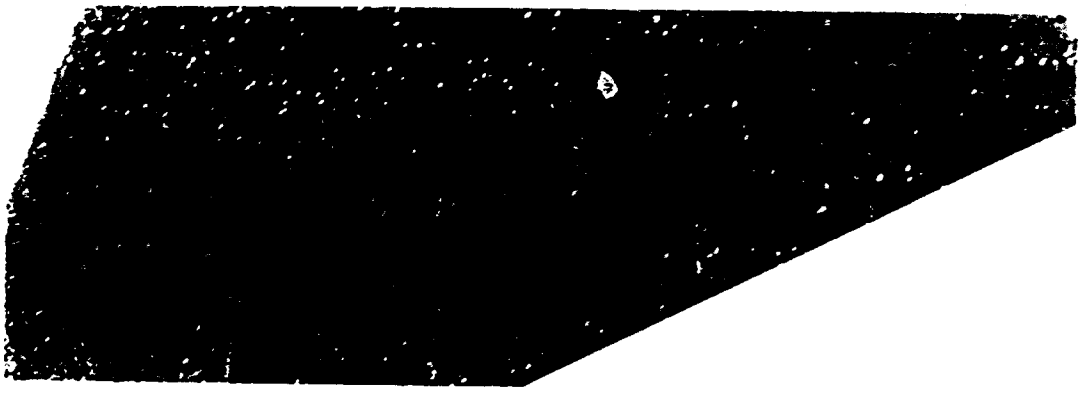

10X

X-RAY TRANSMISSION

26.3

10X

Arthur D Little Inc

26-1

OPTICAL

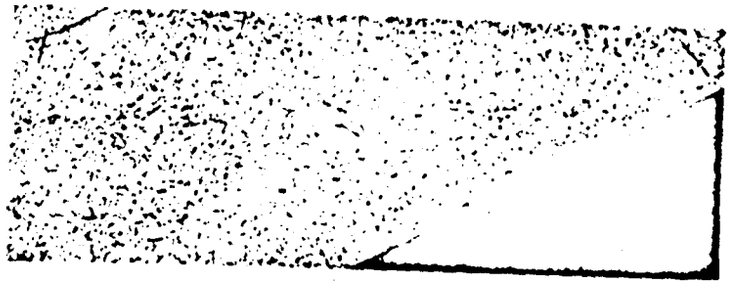

10X

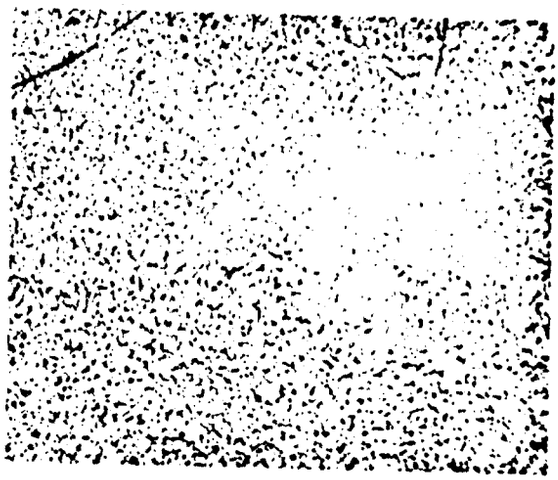

22X

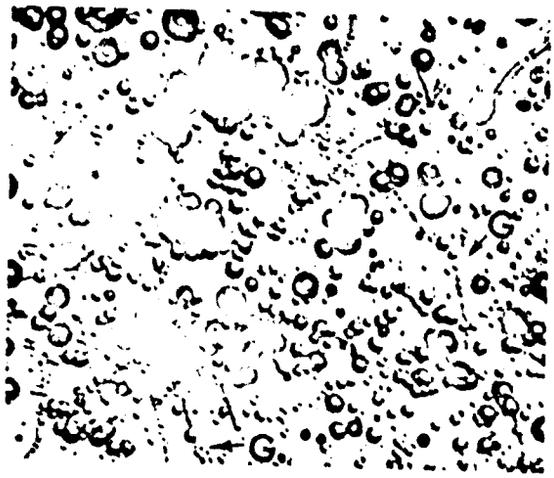

150X

26.2

X-RAY BACK REFLECTION

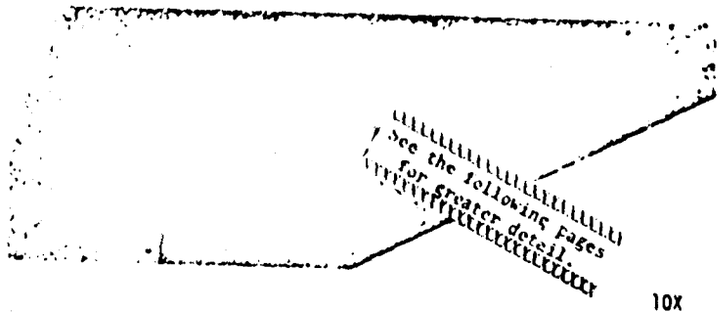

10X

X-RAY TRANSMISSION

26.3

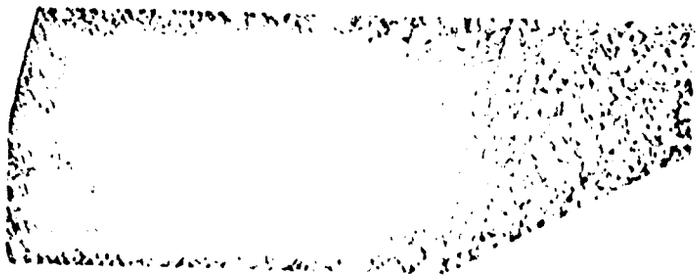

10X

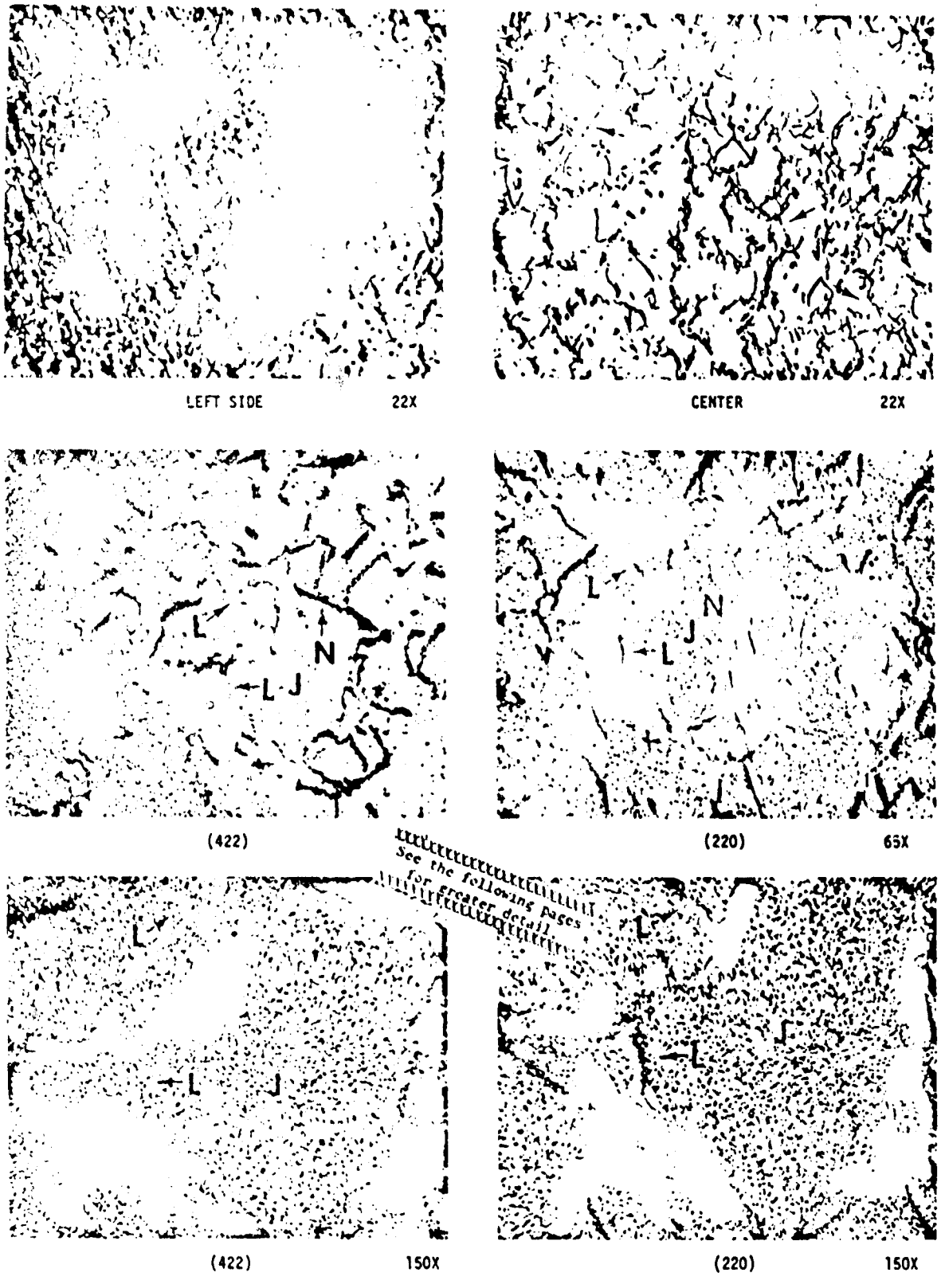

FIGURE 8 OPTICAL, BACK REFLECTION AND TRANSMISSION X-RAY TOPOGRAPHS OF A (111)-ORIENTED THIN SECTION OF GaAs FROM SAMPLE No. 2602-10

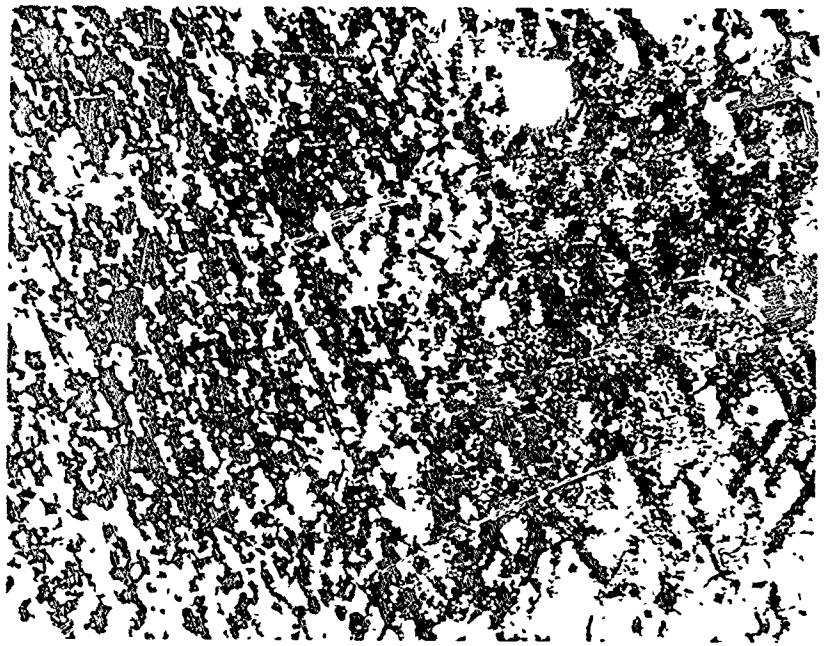

LEFT SIDE 22X

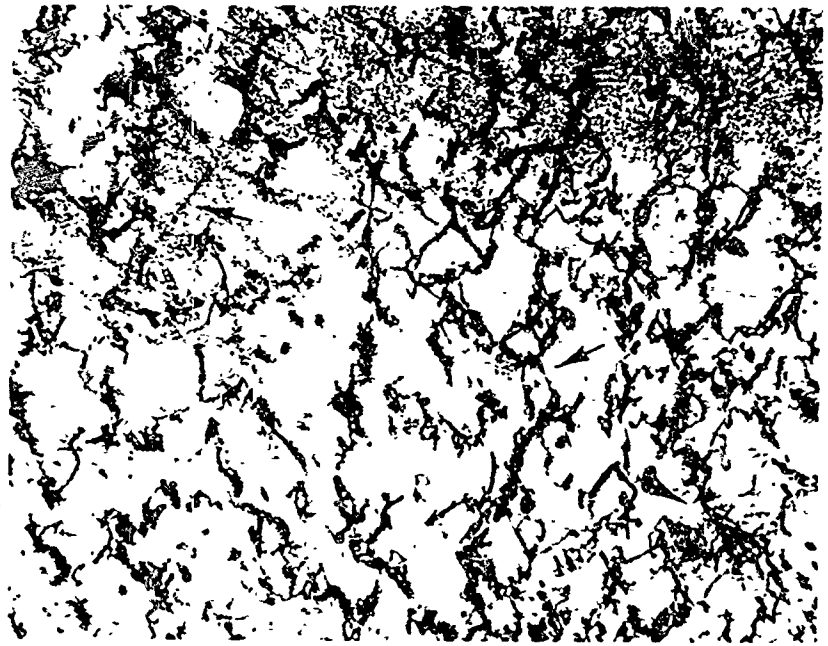

CENTER 22X

(422) 65X

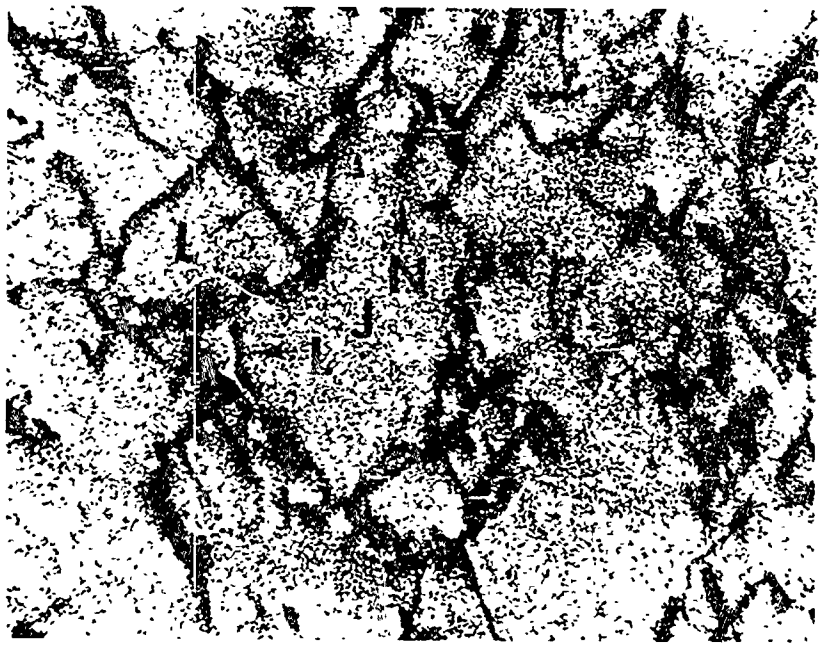

(220) 65X

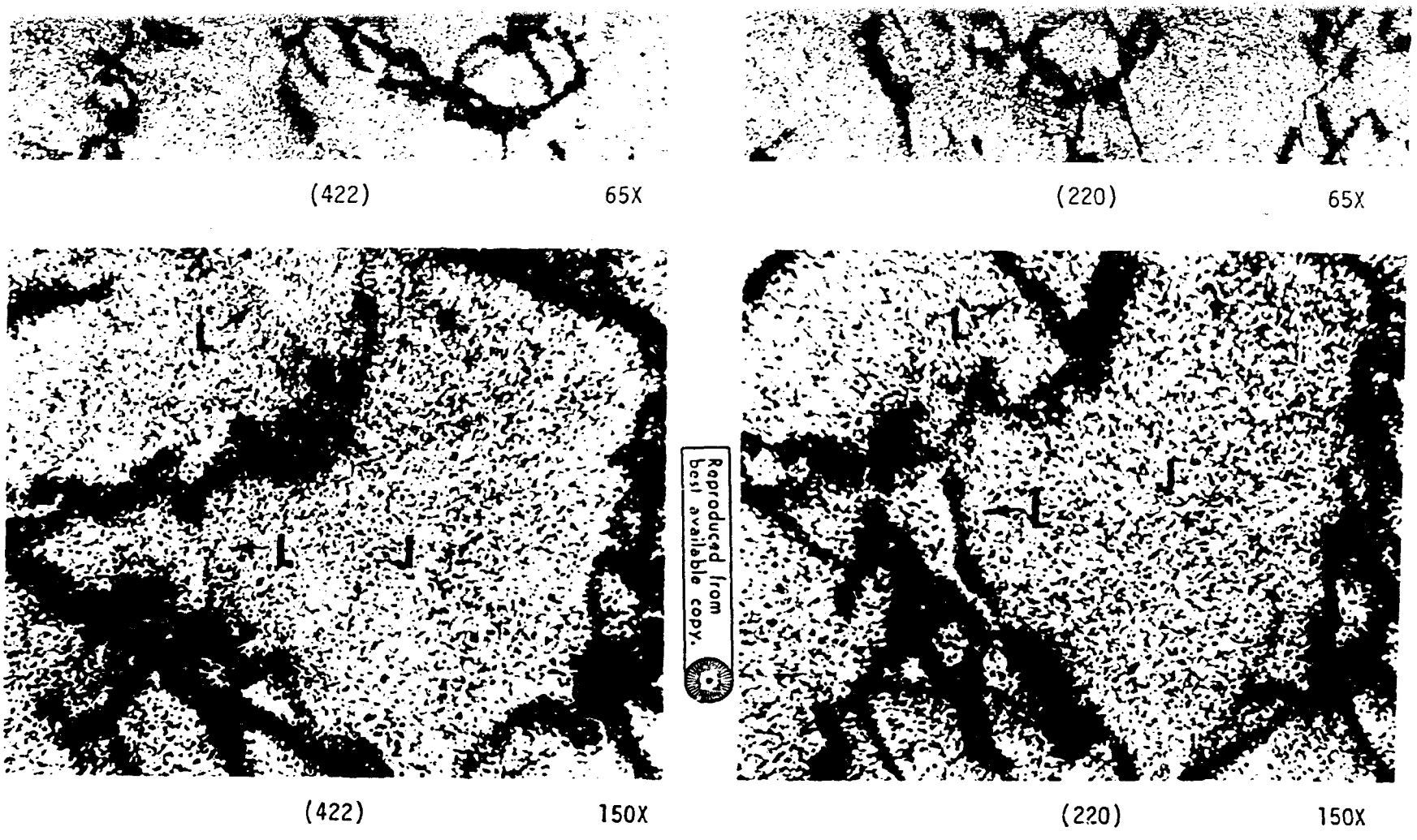

FIGURE 8 OPTICAL, BACK REFLECTION AND TRANSMISSION X-RAY TOPOGRAPHS OF A (111)-ORIENTED THIN SECTION OF GaAs FROM SAMPLE No. 26G2-10

10X

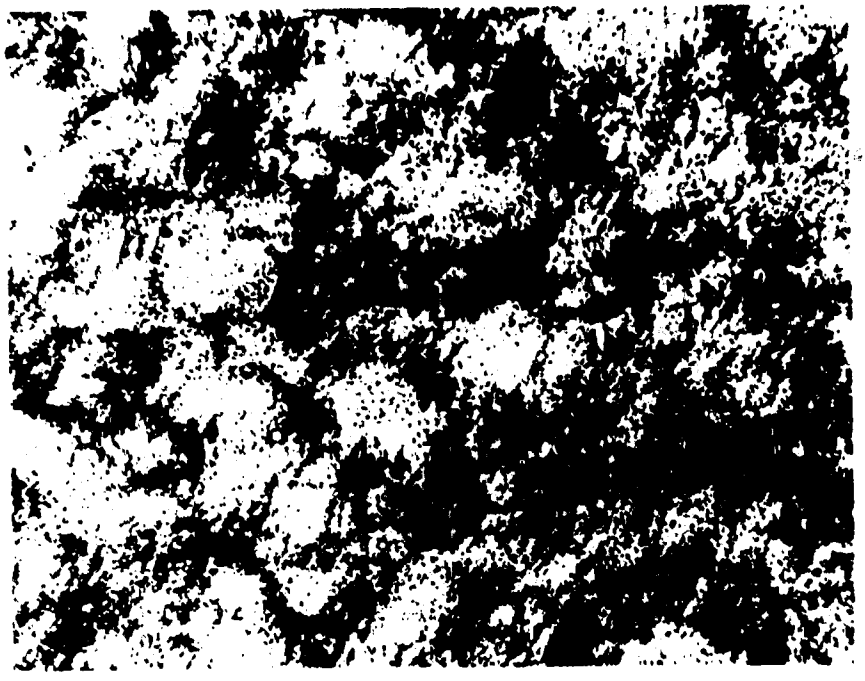

65X

FIGURE 9 TRANSMISSION X-RAY TOPOGRAPHS OF A THIN SECTION OF GaAs FROM SAMPLE NO

28-1

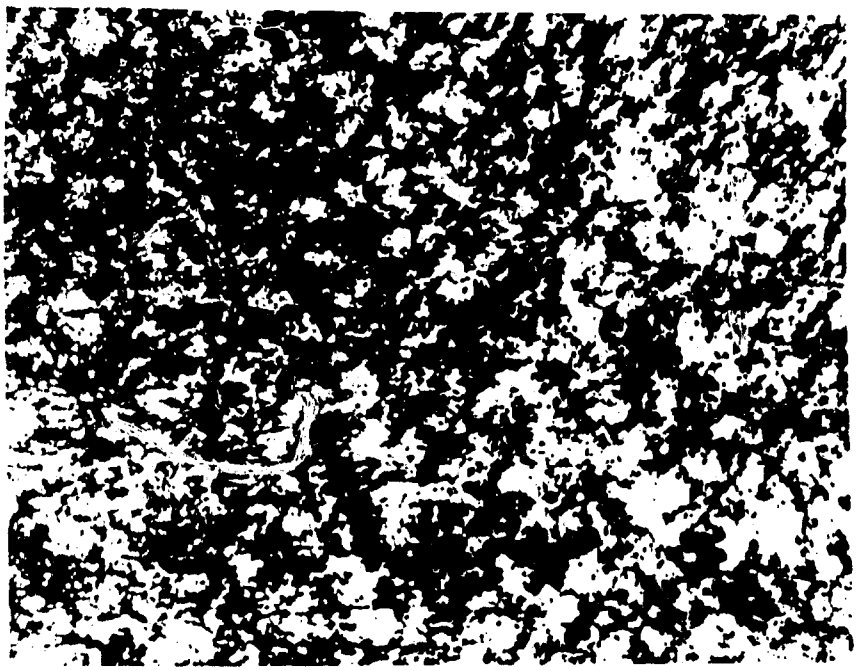

22X

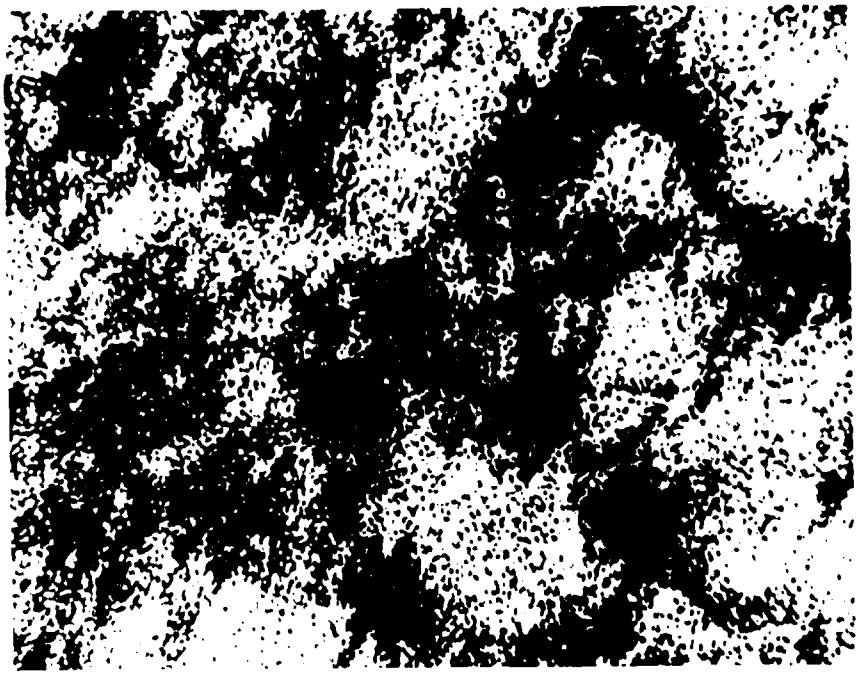

150X

)GRAPHS OF A (111)-ORIENTED
ROM SAMPLE NO. 1860T

10X

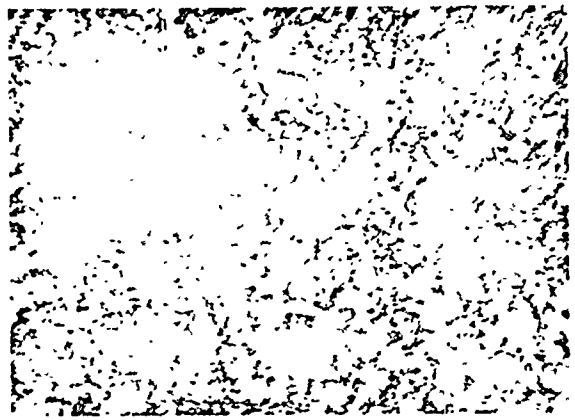

22X

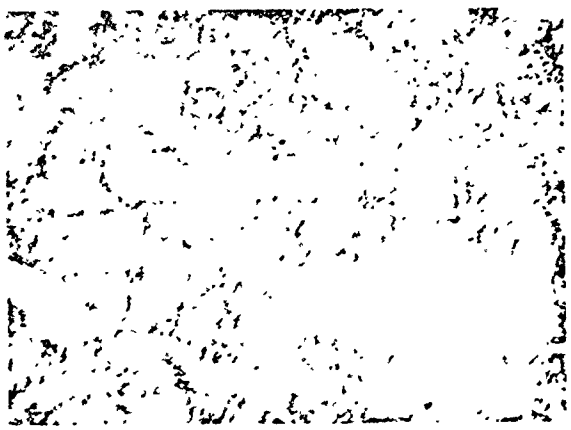

65X

150X

FIGURE 9 TRANSMISSION X-RAY TOPOGRAPHS OF A (111)-ORIENTED THIN SECTION OF GaAs FROM SAMPLE NO. 1860T

28.1

28.3